

# Bistable dynamics of ion homeostasis in ion-based neuron models

Niklas Hübel,<sup>1</sup> Eckehard Schöll,<sup>1</sup> and Markus A. Dahlem<sup>2, a)</sup>

<sup>1)</sup>*Department of Theoretical Physics, Technische Universität Berlin, Germany*

<sup>2)</sup>*Institute for Physics, Humboldt Universität zu Berlin, Berlin, Germany*

(Dated: 14 November 2022)

When neurons fire action potentials, dissipation of free energy is usually not directly considered, because the change in free energy is often negligible compared to the immense reservoir stored in neural transmembrane ion gradients and the long-term energy requirements are met through chemical energy, i.e., metabolism. However, these gradients can temporarily nearly vanish in neurological diseases, such as migraine and stroke, and in traumatic brain injury from concussions to severe injuries. We study biophysical neuron models based on the Hodgkin–Huxley (HH) formalism extended to include time-dependent ion concentrations inside and outside the cell and metabolic energy-driven pumps. For the first time, a minimal model is developed, which resolves a structural instability inherent in this HH extension. We reveal the basic mechanism of a state of free energy-starvation (FES) with bifurcation analyses showing that ion dynamics are bistable for a large range of pump rates. This is interpreted as a threshold reduction of a new fundamental mechanism of ionic excitability that causes a long-lasting but transient FES as observed in pathological states. We can in particular conclude that a coupling of extracellular ion concentrations to a large glial-vascular bath can take a role as an inhibitory mechanism crucial in ion homeostasis, while the  $\text{Na}^+/\text{K}^+$  pumps alone are insufficient to recover from FES. Our results provide the missing link between the HH formalism and activator–inhibitor models that have been successfully used for modeling migraine phenotypes, and therefore will allow us to validate the hypothesis that migraine symptoms are explained by disturbed function in ion channel subunits,  $\text{Na}^+/\text{K}^+$  pumps, and other proteins that regulate ion homeostasis.

## 1. INTRODUCTION

The Hodgkin–Huxley (HH) model is one of the most successful models in mathematical biology<sup>1</sup>. This formalism, i.e., a HH-type model, describes voltage changes across cell membranes that result in excitability. Not only neurons are excitable cells, also myocytes, pancreatic  $\beta$ -cells, and even a plant cell (*Chara corallina*) exhibit excitable dynamics<sup>2–4</sup>. The dynamic range of phenomena includes single action potentials (spikes), periodic spiking, and bursting (slow modulation of spiking). For example, in pancreatic  $\beta$ -cells bursting is induced by a calcium current<sup>4,5</sup>, a more complete treatment of this phenomenon, however, also requires inclusion of  $\text{Na}^+/\text{K}^+$  pumps<sup>6</sup>. The dynamics of ion pumps and accumulating ion concentrations is also crucial for cardiac alternans (periodic beat-to-beat variations) and higher-order rhythms in ischemic ventricular muscle<sup>7–9</sup>. A fundamental property of ion-based models is a structural instability that is related to the linear dependence of the dynamic variables due to a conservation law<sup>10–12</sup>. The phase space structure of such systems can be changed by an arbitrarily small perturbation. In a proper treatment this structural instability can be resolved by eliminating the linearly dependent variables. These augmented HH-type models are also called second-generation HH models<sup>13</sup>.

In the context of certain pathologies of the brain, whose fundamental dynamic structure we study here, we prefer the simpler name ‘ion-based’ models. This indicates that ion concentrations are major dynamical vari-

ables. Their dynamical role in neuron models goes beyond merely modulating spiking activity. Ion dynamics can lead to a completely new type of ionic excitability and bistability, that is, the phenomena of so-called ‘spreading depolarizations’ and ‘anoxic depolarization’, respectively. These depolarized states of neurons are related to migraine, stroke, brain injury and brain death, that is, to pathologies of the brain in which a transient or permanent break-down of the transmembrane potential occurs<sup>14,15</sup>. Another even more characteristic property of this ‘twilight state close to death’<sup>16</sup> are the nearly completely flat transmembrane ion gradients. The almost break-down of both membrane potential and ion gradients, i.e., Nernst potentials, together cause a nearly complete release of the Gibbs free energy, that is, the thermodynamic potential that measures the energy available to the neurons for operation. We hence refer to this state as a state of free energy-starvation (FES).

The object of this study is to clarify quantitatively the detailed ion-based mechanisms, in particular the time-dependent potentials. From the classical HH perspective, the dynamics of the Nernst potentials (also called ‘reversal potentials’) are of interest. However, we want to stress that due to this extension, the physical or rather thermodynamical perspective is important, which goes beyond the interpretation and use of equivalent electrical circuits in membrane physiology (see discussion).

In fact, the phenomenon of spreading depolarization has been described by ion-based models<sup>17–23</sup>, but, interestingly, none of these studies take care of—or even seem to have noted—the structural instability that was described for excitable myocytes and pancreatic  $\beta$ -cells with variable ion concentrations<sup>10,11,24</sup>. Ion-based mod-

<sup>a)</sup>Corresponding author; dahlem@physik.hu-berlin.de

els have also been used to study the modulating effect of ion concentrations in seizure activity<sup>25,26</sup> and in spontaneous excitation patterns in myelinated axons with injury-like membrane damaging conditions (e.g., caused by concussions)<sup>27,28</sup> in each case without considering the structural instability.

Our bifurcation analysis of minimal biophysical ion-based models reveals that ion dynamics cause bistability for a large range of pump rates. Bistability of a polarized and a depolarized state has also been found in the original HH model for a fixed high extracellular potassium concentration<sup>29</sup>. In this paper, however, we show bistability of states with extremely different ion concentrations. This is interpreted as a model that describes a threshold reduction of a mechanism that leads to ionic excitability in form of spreading depolarizations. In other words, we can conclude that an important inhibitory mechanism to describe ion homeostasis such as glial buffering or diffusive regulation of extracellular ion concentrations plays a crucial role in ion homeostasis and the  $\text{Na}^+/\text{K}^+$  pumps alone are insufficient to recover from free energy-starved states. This has been validated by demonstrating the robustness of the results in a large variety of minimal ion-based models, which all consistently show this insufficiency of  $\text{Na}^+/\text{K}^+$  pumps.

## 2. MINIMAL ION-BASED MODEL

A simple ion-based neuron model can be obtained as a natural extension of the Hodgkin-Huxley (HH) model<sup>1</sup>. In HH, single neuron dynamics are described in terms of an electrically active membrane carrying an electric potential  $V$ , and the three gating variables  $n$ ,  $m$  and  $h$  that render the system excitable. Ion species included are sodium, potassium and an unspecified ion carrying a leak current, which can be attributed to chloride in our extended model. The number of independent gating variables can be reduced to one by assuming a functional relation between  $h$  and  $n$  and eliminating  $m$  adiabatically. The rate equations for the remaining variables are

$$\frac{dV}{dt} = -\frac{1}{C_m}(I_{\text{Na}^+} + I_{\text{K}^+} + I_{\text{Cl}^-} - I_{\text{app}}), \quad (1)$$

$$\frac{dn}{dt} = \frac{n_\infty - n}{\tau_n}, \quad (2)$$

with ion currents expressed in terms of conductances  $g_{\text{ion}}^{l,g}$  and Nernst potentials  $E_{\text{ion}}$  (for  $\text{ion} = \text{K}$ ,  $\text{Na}$  and  $\text{Cl}$ ):

$$I_{\text{Na}^+} = (g_{\text{Na}}^l + g_{\text{Na}}^g m^3 h) \cdot (V - E_{\text{Na}}), \quad (3)$$

$$I_{\text{K}^+} = (g_{\text{K}}^l + g_{\text{K}}^g n^4) \cdot (V - E_{\text{K}}), \quad (4)$$

$$I_{\text{Cl}^-} = g_{\text{Cl}}^l \cdot (V - E_{\text{Cl}}). \quad (5)$$

They are complemented by the two gating constraints

$$m = m_\infty(V), \quad (6)$$

$$h = h_{\text{sig}}(n). \quad (7)$$

The relaxation time and the asymptotic value of the gating variable  $n$  are given by  $\tau_n(V)$  and  $n_\infty(V)$ , respectively. For no applied current ( $I_{\text{app}} = 0$ ) the HH model has a stable fixed point at  $V = -68$  mV. For details see the Appendix. A complete set of parameters and derived quantities is found in tab. III.

While in the original HH model ion concentrations are model parameters, in ion-based modeling intra- and extracellular ion concentrations become dynamical variables, which causes the Nernst potentials to be dynamic. The HH formalism can straightforwardly be extended to make ion concentrations dynamic since currents induce ion fluxes. However, under those equilibrium conditions found in HH neither  $I_{\text{K}^+} = 0$  nor  $I_{\text{Na}^+} = 0$ . Hence we need to include ion pumps<sup>11</sup> to make sure that the rate of change in ion concentration inside the cell ( $i$ ) and extracellular ( $e$ ) can vanish in the resting state ( $\dot{N}a_{i/e} = \dot{K}_{i/e} = \dot{C}l_{i/e} = 0$ ). Note that we omit the square brackets on the ion concentrations and simply write, for example,  $K_i$  and  $K_e$ , or  $K_{i/e}$  if we mean both potassium concentrations. The rate equations for ion concentrations in the intracellular space (ICS) are then

$$\frac{dNa_i}{dt} = -\frac{\gamma}{\omega_i}(I_{\text{Na}^+} + 3I_p), \quad (8)$$

$$\frac{dK_i}{dt} = -\frac{\gamma}{\omega_i}(I_{\text{K}^+} - 2I_p), \quad (9)$$

$$\frac{dCl_i}{dt} = +\frac{\gamma}{\omega_i}I_{\text{Cl}^-}. \quad (10)$$

The factor  $\gamma$  converts currents to ion fluxes and depends on the membrane surface  $A_m$  and Faraday's constant  $F$ :

$$\gamma = \frac{A_m}{F}, \quad (11)$$

Dividing the ion fluxes by the ICS volume  $\omega_i$  gives the change rates for the ICS ion concentrations. The pump current  $I_p$  represents the ATP-driven exchange of ICS sodium with potassium from the extracellular space (ECS) at a 3/2-ratio. It increases with the ICS sodium and the ECS potassium concentration. Chloride is not pumped. We are using the pump model from<sup>25,26</sup>:

$$I_p(Na_i, K_e) = \rho \left( 1 + \exp\left(\frac{25 - Na_i}{3}\right) \right)^{-1} \left( 1 + \exp(5.5 - K_e) \right)^{-1}, \quad (12)$$

where  $\rho$  is the maximum pump current. As a consequence of mass conservation ion concentrations in the ECS can be computed from those in the ICS:

$$\text{ion}_e = \text{ion}_e^{(0)} + \frac{\omega_e}{\omega_i}(\text{ion}_i^{(0)} - \text{ion}_i),$$

with the ECS volume  $\omega_e$ . Superscript zero indicates initial values. Since all types of transmembrane currents, i.e., also the pumps, must be included in eq. (1) for the

membrane potential, we have to add the net pump current  $I_p$ :

$$\frac{dV}{dt} = -\frac{1}{C_m}(I_{Na^+} + I_{K^+} + I_{Cl^-} + I_p - I_{app}) . \quad (13)$$

The rate equations for the ion-based model are thus given by eqs. (2), (8)–(10), (13). These rate equations are complemented by the gating constraints eqs. (6), (7) and the mass conservation constraints

$$Na_e = Na_e^{(0)} + \frac{\omega_e}{\omega_i}(Na_i^{(0)} - Na_i) , \quad (14)$$

$$K_e = K_e^{(0)} + \frac{\omega_e}{\omega_i}(K_i^{(0)} - K_i) , \quad (15)$$

$$Cl_e = Cl_e^{(0)} + \frac{\omega_e}{\omega_i}(Cl_i^{(0)} - Cl_i) . \quad (16)$$

Dynamic ion concentration imply that the Nernst potentials in eqs. (3)–(5) are now dynamic (see eq. (36) in the Appendix). The additional parameters of the ion-based model are listed in tab. I. Because of the extremely small value of  $\gamma$  the membrane dynamics, i.e., the dynamics of  $V$  and  $n$ , are five orders of magnitude faster than the ion dynamics.

A consequence of this large timescale separation is that the system will attain a Donnan equilibrium when the pumps break down. The Donnan equilibrium is a thermodynamic equilibrium state (not to be confused with merely a fixed point, though it is one) that is reached for electroneutral ion exchange across a semipermeable membrane. Since we have not explicitly included large impermeable anions inside the cell, this is at first surprising. For no applied currents and  $I_p = 0$  the ion rate equations imply that an equilibrium requires all Nernst potentials to be equal, so ion concentrations will adjust accordingly. However, eqs. (8)–(10) and (13) imply the following constraint on the ICS charge concentration  $Q_i$ :

$$\Delta Q_i := \Delta Na_i + \Delta K_i - \Delta Cl_i = \frac{C_m \gamma}{\omega_i} \Delta V , \quad (17)$$

where  $\Delta$  denotes the difference between the initial and final value of a variable. Since  $\gamma$  is very small, changes in ion concentrations must practically satisfy electroneutrality. This condition plus the equality of all Nernst potentials define the Donnan equilibrium, so we see that it is contained in our model as the limit case with no pumps and no applied currents.

In this extension of the HH model the ion dynamics makes Nernst potentials time-dependent. The simultaneous effect of a diffusive and an electrical force acting on a solution of ions is described more accurately by the Goldman–Hodgkin–Katz (GHK) equation though. Nevertheless we prefer Nernst currents, because this formulation allows us to use well-established conductance parameters so that the model is completely defined by empirically estimated parameters. In Sec. 4.1 we will see how GHK currents can be modelled and that the qualitative dynamical behaviour of the system is not affected.

TABLE I. Model parameters for ion-based model only

name	value & unit	description
$\omega_i$	2.16 $\mu\text{m}^3$	volume of ICS
$\omega_e$	0.72 $\mu\text{m}^3$	volume of ECS
$F$	96.485 C/mMol	Faraday's constant
$A_m$	0.922 $\mu\text{m}^2$	membrane surface
$\gamma$	9.556e-5 ( $\frac{\text{mMol/l}}{\text{msec}})/(\frac{\mu\text{A}/\text{m}^2}{\mu\text{m}^3})$	conversion factor
$\rho$	5.25 $\mu\text{A}/\text{cm}^2$	max. pump current

### 3. PHASE SPACE ANALYSIS OF ION-BASED MODEL

In the ion-based model introduced above current pulses can still initiate voltage spikes (not shown). However, extremely strong pulses can drive the system away from the physiological equilibrium to a second stable fixed point that is strongly depolarized (see fig. 1(a)). This is a new dynamical feature. The depolarized state can also be reached when the ion pumps are temporarily switched off (see fig. 1(b)). Apart from the depolarization this state is characterized by almost vanishing ion gradients. This free energy-starvation (FES) is reminiscent of the Donnan equilibrium. Extracellular potassium is increased from 4 to more than 40 mMol/l while the extracellular sodium concentration is reduced from 120 to less than 30 mMol/l. The gated ion channels are mostly open (potassium activation  $n$  is 60%), and it is no longer possible to initiate voltage spikes. In this section we will present a phase space analysis of the model and derive conditions for the observed bistability of a physiological equilibrium and a state of FES.

#### 3.1. Symmetry of the ion-based model

Before a bifurcation analysis can be done we need to discuss a conservation law (symmetry) of eqs. (8)–(10), (13). The model is degenerate which renders the system structurally unstable. To see this note that for  $I_{app} = 0$  the rate equations satisfy

$$C_m \frac{dV}{dt} = \frac{\omega_i}{\gamma} \left( \frac{dNa_i}{dt} + \frac{dK_i}{dt} - \frac{dCl_i}{dt} \right) , \quad (18)$$

i.e., the variables are linearly dependent, so the determinant of the Jacobian is always zero and hence the system is nowhere hyperbolic. The phase space structure of such systems can be changed with arbitrarily small perturbations which is why they are called structurally unstable<sup>30</sup>. As a consequence we cannot apply standard continuation techniques of bifurcation theory to analyse the phase space, because these require hyperbolicity almost everywhere. The physiological view on the instability should be as follows. Assume that the system is in its physiological equilibrium and then apply a constant current  $I_{app}$  to the voltage rate eq. (13). Then eqs. (8)–(10) and (13) imply that the equilibrium conditions  $\dot{V} = 0$  and

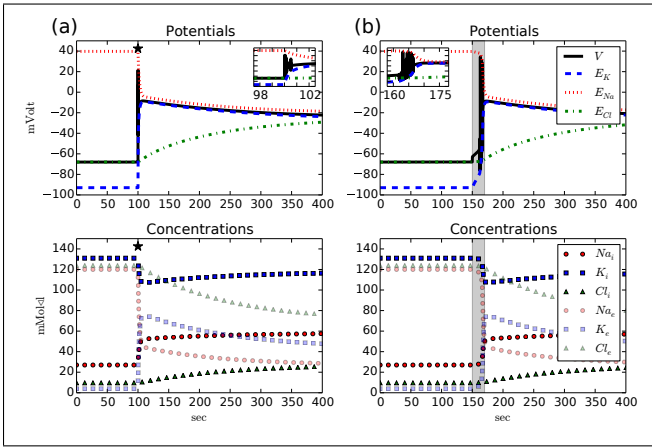


FIG. 1. Upper panels: membrane and Nernst potentials, lower panel: ion concentrations vs time. **(a)** Response of the model to a 0.5 sec long sodium current pulse with amplitude  $150 \mu\text{A}/\text{cm}^2$  (marked by the black star). The pulse causes voltage spiking that stops in a strongly depolarized state (see blow-up inset). The membrane potential  $V$  takes a final value of about  $-25$  mV (upper panel). The ion gradients, i.e., the differences between intra- and extracellular ion concentrations, reduce drastically during the stimulation and slowly adjust to a new fixed point after a couple of hundreds of seconds (lower panel). **(b)** Switching off the ion pump for 20 sec (indicated by the light grey interval) causes similar dynamics. The membrane depolarization and dissipation of ion gradients is a bit slower than for (a). After the pump is switched on again the system attains the same fixed point as in (a).

$\dot{K}_i = \dot{Na}_i = \dot{Cl}_i = 0$  are contradictory, so the equilibrium will vanish even for arbitrarily small currents. In fact, the system will evolve in a highly non-physiological manner with  $K_i$ ,  $Na_i$  and  $Cl_e$  tending to zero. Note that a current pulse of finite length does not lead to the same problem, because after a stimulus the system will have a fixed point again. The mathematical solution is to exploit the symmetry and thereby reduce the number of dynamical variables. We can, for example, choose to eliminate  $V$  and express it in terms of the ICS ion concentrations rather than treating  $V$  as an independent dynamical variable<sup>11</sup>:

$$\begin{aligned} \frac{d}{dt} \left( V - \frac{\omega_i}{C_m \gamma} (Na_i + K_i - Cl_i) \right) &= 0 \\ \Rightarrow V &= V^{(0)} + \\ &\frac{\omega_i}{C_m \gamma} \left( Na_i - Na_i^{(0)} + K_i - K_i^{(0)} - Cl_i + Cl_i^{(0)} \right) \end{aligned}$$

The reduced system is then structurally stable. The physiological view on this reduction is simply that the possibility of unspecified applied currents is ruled out. For instance, a perturbation on eq. (8) should be interpreted as a sodium current. The above constraint describes the simultaneous effect on  $V$ . It would be equivalent to apply perturbations to eq. (8) and eq. (13) consistently to

model the full effect of an applied sodium current, so the additional constraint should be seen as a consistency condition. Note that stimulation with unspecified and specified current pulses can hardly be distinguished in numerical simulations. (The curves in fig. 1(a) were computed for a sodium current pulse.) In fact, for the bifurcation analysis presented in this paper we have eliminated  $Na_i$  rather than  $V$  for numerical reasons, which is equivalent as long as no currents are applied. That means that we have replaced rate eq. (8) by the following constraint:

$$Na_i = Na_i^{(0)} - K_i + K_i^{(0)} + Cl_i - Cl_i^{(0)} + \frac{C_m \gamma}{\omega_i} (V - V^{(0)}) \quad (19)$$

The model is then defined by the rate eqs. (2), (9), (10) and (13) and the constraint eqs. (6), (7), (14)–(16) and (19).

### 3.2. Bifurcation analysis

We have used the continuation tool AUTO to follow the polarized fixed point of the system under variation

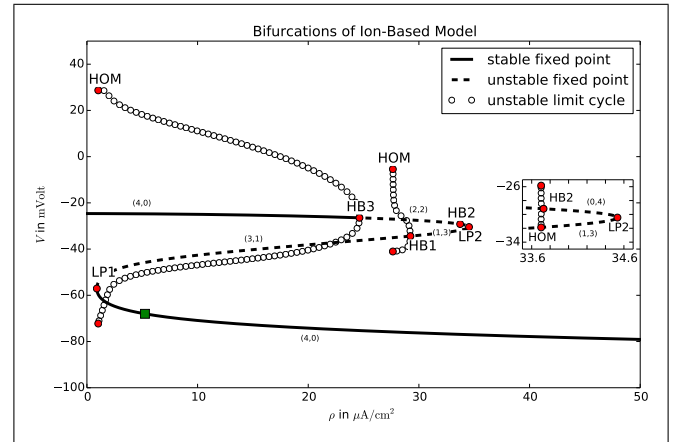


FIG. 2. Bifurcation diagram of the ion-based model. Bifurcations are marked by red circles, the physiological equilibrium by a green square. Following the z-shaped fixed point characteristic from below there are two saddle-node bifurcations (limit point, LP) at  $\rho = 0.894006 \mu\text{A}/\text{cm}^2$  and  $\rho = 34.5299 \mu\text{A}/\text{cm}^2$ , and three subcritical Hopf bifurcations (HB) at  $\rho = 29.2336 \mu\text{A}/\text{cm}^2$ ,  $\rho = 33.7285 \mu\text{A}/\text{cm}^2$  and  $\rho = 24.6269 \mu\text{A}/\text{cm}^2$ . The limit cycles created in HB1, HB2 and HB3 disappear in homoclinic bifurcations (HOM) at  $\rho = 27.6463 \mu\text{A}/\text{cm}^2$ ,  $\rho = 3.37027 \mu\text{A}/\text{cm}^2$  and  $\rho = 1.024291 \mu\text{A}/\text{cm}^2$ , respectively. The second LP and the second HB together with the HOM of limit cycles occur in a very narrow parameter range (see blow-up inset). The number of stable ( $n_-$ ) and unstable ( $n_+$ ) directions of the fixed point is indicated by the  $(n_-, n_+)$ -tuples. There is bistability of a physiological state and a depolarized state with largely reduced ion concentration gradients between  $\rho = 8.94006 \mu\text{A}/\text{cm}^2$  and  $\rho = 24.6269 \mu\text{A}/\text{cm}^2$ .

of the maximal pump rate  $\rho$ . Stability changes and the creation of stable or unstable limit cycles are detected by the software which helps us to interpret the dynamical behaviour. For a better overview we will extend our bifurcation analysis even beyond the physiologically relevant range. The full bifurcation diagram is presented in fig. 2.

In the  $(\rho, V)$ -plane the fixed point continuation yields a smooth z-shaped curve where unstable sections are dashed. The physiological equilibrium is marked by a green square. For higher pump rates the equilibrium remains stable and becomes slightly hyperpolarized. If  $\rho$  is decreased the physiological equilibrium collides with a saddle point at  $\rho_{LP1} = 0.894006 \mu\text{A}/\text{cm}^2$  in a saddle-node bifurcation (limit point, LP). In a LP the stability of a fixed point changes in one direction (zero-eigenvalue bifurcation). Thus after LP1 the fixed point is a saddle point with one unstable direction. In a Hopf bifurcation (HB) at  $\rho_{HB1} = 29.2336 \mu\text{A}/\text{cm}^2$  two more directions become unstable. Via another LP at  $\rho_{LP2} = 34.5299 \mu\text{A}/\text{cm}^2$  the last stable direction switches to unstable and the saddle becomes an unstable node. In HBs at  $\rho_{HB2} = 33.7285 \mu\text{A}/\text{cm}^2$  and  $\rho_{HB3} = 24.6269 \mu\text{A}/\text{cm}^2$  the fixed point becomes a saddle and a stable depolarized focus, respectively. The stability is indicated by the  $(n_-, n_+)$ -tuples along the fixed point curve with  $n_-, n_+$  denoting the number of stable and unstable directions.

In every HB a limit cycle is created. Our model only contains unstable limit cycles that are created in subcritical HBs. In the diagram they are represented by their extremal  $V$  values. Such unstable limit cycles are not directly observable, but in the bistable regime they can play a role for the threshold behaviour for the transition from one fixed point to the other. All limit cycles in the model disappear in homoclinic bifurcations (HOM). In a HOM a limit cycle collides with a saddle. When it touches the saddle it becomes a homoclinic cycle of infinite period. After the bifurcation the limit cycle does not exist any more. The limit cycles created in HB1, HB2 and HB3 disappear in HOMs at  $\rho = 27.6463 \mu\text{A}/\text{cm}^2$ ,  $\rho = 3.37027 \mu\text{A}/\text{cm}^2$  and  $\rho = 1.024291 \mu\text{A}/\text{cm}^2$ . The limit cycle emanating from HB1 collides with the upper (i.e., less polarized) saddle, for the other two HOMs the situation is clear, because there is only one saddle available. Since the limit cycles are all unstable these bifurcation details are physiologically irrelevant, but mentioned for completeness.

This bifurcation analysis shows that our model is bistable for a large range of pump rates  $\rho_{LP1} < \rho < \rho_{HB3}$ . Strongly depolarized and electrically inactive states of neurons with nearly vanishing ion concentration gradients have been reported in pathological states<sup>14,16</sup>, but such free energy-starvation (FES) is not stable. Bistable systems can be interpreted as a threshold reduction in which the inhibitory mechanism of excitability is eliminated. We refer the reader to the discussion in Sec. 5.

## 4. ROBUSTNESS OF RESULTS

The ion-based model we have analysed so far has been motivated as a natural extension of the Hodgkin–Huxley membrane model. However, there are different variants of ion-based models<sup>17–23,25,26</sup> that use different pump and current models, ion content, and ion channels. We will hence address the question how general our results are in this respect. Furthermore we vary the geometry-dependent parameters (membrane surface and interstitial volume fraction) continuously to test their effect on the phase space, too.

### 4.1. Model variants

In Sec. 2 we noted crossmembrane currents are more accurately described as GHK rather than Nernst currents, even though we prefer the latter. It is hence important to check which difference the choice of current model makes. To generalize the Nernst currents in eqs. (3)–(5) to GHK currents we assume that both models have the same steady state currents under physiological equilibrium conditions. The GHK version of the sodium current is

$$I_{Na^+}^{GHK} = (P_{Na}^l + P_{Na}^g m^3 h) \cdot F \cdot \frac{V}{26.64} \cdot \frac{Na_i - Na_e \exp(-V/26.64)}{1 - \exp(-V/26.64)} \quad (20)$$

with membrane permeabilities  $P_{Na}^l$  and  $P_{Na}^g$  instead of conductances. To compute these permeabilities we set the GHK current equal to its Nernstian counterpart

$$I_{Na^+} = (g_{Na}^l + g_{Na}^g m^3 h) \cdot (V - E_{Na}) \quad (21)$$

for the equilibrium conditions given in tab. III. This leads to a common conversion factor from conductances  $g_{Na}^{l,g}$  to permeabilities  $P_{Na}^{g,l}$ . With this ansatz we obtain conversion factors for the three different ion species that lead to the conductances listed in tab. II.

There is also a certain freedom in the choice of a pump model. It is a general feature of  $\text{Na}^+/\text{K}^+$  pumps that their activity is enhanced by the elevation of ECS potassium and ICS sodium. Still different models exist, and to investigate the role of the particular pump model we replace the pump from eq. (12), now referred to as  $I_{p,A}$ , with the following one from<sup>17</sup>:

$$I_{p,B}(Na_i, K_e) = \rho_B \left(1 + \frac{3.5}{K_e}\right)^{-2} \left(1 + \frac{10}{Na_i}\right)^{-3} \quad (22)$$

In order to retain the equilibrium at  $V = -68$  mV we have to set the maximum pump current to  $\rho_B = 5.72 \mu\text{A}/\text{cm}^2$ . This is slightly higher than the previous pump value ( $\rho_A = 5.25 \mu\text{A}/\text{cm}^2$ ), but in the same range.

From the HH rate equations (see Sec. 2 and Appendix) it is obvious that the chloride leak current stabilizes the

equilibrium membrane potential. To test its stabilizing effect in the context of ion-based modeling we compare models that either do or do not contain this current. We are further interested in the question whether membrane excitability and ion bistability are related. Therefore also the effect of in- and excluding active ion channels is tested.

In this section we will only discuss fixed points and their stability, but not the unstable limit cycles belonging to HBs. In fig. 3 the fixed point continuation curves for all combinations of current model (Nernst or GHK), pump choice ( $I_{p,A}$  or  $I_{p,B}$ ) and the respective in- and exclusion of chloride and active ion channels channel are shown. Each panel (a)–(d) contains all continuation curves for a given choice of pump and current model. For those models that are bistable for certain pump rates an overview of the different dynamical regimes is presented in fig. 4. It shows the parameter ranges for bistability and for monostability of a physiological state or FES.

The most striking result of this bifurcation analysis is that this bistability occurs in all models with gated ion channels, but not in any model with only leak channels (grey-shaded graphs in the insets of fig. 3). The comparison of any model with active gates and its leak-only counterpart shows that whenever the physiological equilibrium of the first one exists it is identical to the equilibrium of the latter one. While the physiological state disappears in a LP for all bistable models at small pumping, the fixed points of the leak models remain stable, but depolarize drastically for further decreasing pump rates until the Donnan equilibrium for  $\rho_{A,B} = 0$  is reached. The absence of the second fixed point in leak-only models is plausible if we consider fig. 1 again. The depolarized state is characterized by large ion concentrations  $K_e$  and  $Na_i$  which implies an increased pump current (see eq. (12)). Since the differences between the Nernst potentials and the membrane potential are even smaller in the depolarized state, higher, hence gated, conductances are required to compensate for the pump currents and maintain the depolarized state. Besides the requirement of active ion channels, the bistability is a very robust feature of these simple ion-based models.

Let us now consider the effect of the different model features on the minimal physiological pump rate, i.e., the pump rate required for a stable physiological fixed point, and the recovery pump rate that destabilizes the depolarized state of FES and allows the neuron to return to physiological conditions. These rates are the lower and upper limit of the bistable regime, and low values are physiologically desirable.

In fig. 4 we see that pump model A, GHK currents and chloride each lead to a lower minimal physiological (see the inset) and a lower recovery pump rate than pump model B, Nernst currents and the exclusion of chloride. Quantitative differences should be noted, though. The inset of fig. 4 shows that all models with pump A have lower minimal physiological pump rates than models with pump B. So the stability of the physiological equilibrium

with respect to pump strength reduction depends mostly on the choice of pump. On the other hand four of the five lowest recovery pump rates are from models that include chloride. In fact, it is only the combination of both, the GHK current model and pump A, that make the recovery threshold of the chloride excluding model 7 slightly lower than that of the chloride including model 2. However, one should note that even the lowest recovery pump rate is as high as  $\rho = 14.3 \mu\text{A}/\text{cm}^2$  (model 8). This is still an almost threefold increase of the normal rate. So even if we assume pump enhancement due to additional mechanisms, for example increased cerebral blood flow, the threshold for recovery from FES seems to be too high. Thus it is true for a large class of ion-based neuron models that realistic neuronal homeostasis cannot rely on  $\text{Na}^+/\text{K}^+$ -ATPase alone, but rather on a combination of ion pumps and further regulation mechanisms like glial buffering.

There is another effect of chloride to be pointed out. In fig. 3 we see that it raises the Donnan equilibrium potential (see potentials at  $\rho = 0 \mu\text{A}/\text{cm}^2$ ) significantly. To understand this effect note that without chloride electroneutrality forces the sum of  $\Delta K_e$  and  $\Delta Na_e$  to be zero, while the presence of the decreasing anion species  $Cl_e$  implies  $\Delta(K_e + Na_e) < 0$ . According to eq. (36) this leads to lower Donnan equilibrium Nernst potentials  $E_K$  and  $E_{Na}$ , and consequently to a lower membrane potential. Since the conditions of FES for physiological pump rate values are very close to the Donnan equilibrium, this depolarized fixed point is shifted in the same way.

The effect of the current model on the two characteristic pump rates is less pronounced than that of chloride or the pump choice. It lowers the minimal physiological rate more than chloride, but not as much as a pump change from model B to A. Its effect on the recovery threshold is the weakest. In general a realistic neuron model should contain chloride, active ion channels and GHK currents. However, since the current model has a rather weak effect on the phase space structure we still prefer the Nernst model over GHK for further investigations.

#### 4.2. Variation of membrane surface and interstitial volume fraction

After the overview of different variants of ion content, ion channels, pumps and current models we finally address the role of the neuron geometry. Therefore we vary the membrane surface and the interstitial volume fraction in the model from Sec. 2. For the surface variation we introduce the relative surface size parameter  $\chi_A$  and replace  $A_m$  with  $A_m\chi_A$  which implies the replacement (see eq. (11))

$$\gamma \rightarrow \gamma\chi_A$$

wherever  $\gamma$  occurs, i.e., in eqs. (9), (10) and (19). The interstitial volume fraction, typically denoted as  $f$ , is de-

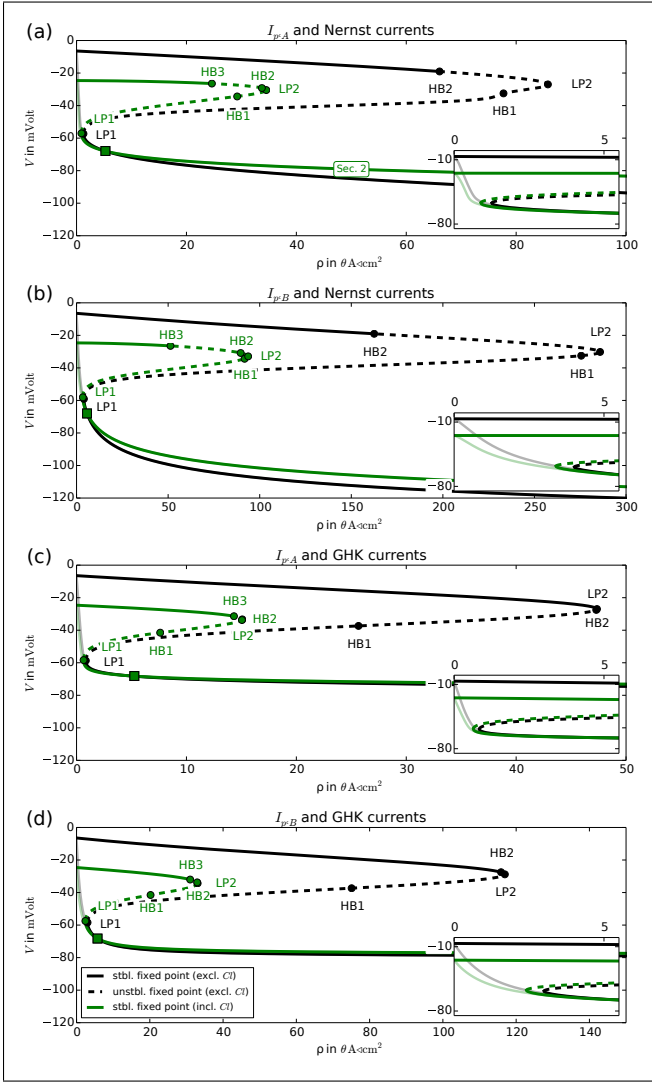


FIG. 3. Bifurcation diagrams of fixed points for different models. The effects of chloride and active ion channels are compared for each of the four possible pump (A vs B) and current model (Nernst vs GHK) combinations. The physiological equilibrium for normal pump rates ( $\rho_A = 5.25 \mu\text{A}/\text{cm}^2$  and  $\rho_B = 5.72 \mu\text{A}/\text{cm}^2$ ) is marked by a green square. The value is the same with and without chloride or active channels. Insets show the bifurcation diagrams for low pump rates ( $\rho_{A,B} < 5 \mu\text{A}/\text{cm}^2$ ). Fixed point lines for models without active ion channels are shaded (see insets). Note the different scales on the main figures, insets are for the same range in each panel.

finned as

$$f := \frac{\omega_e}{\omega_{tot}} \Rightarrow \omega_e = f\omega_{tot} \quad \text{and} \quad \omega_i = (1-f)\omega_{tot},$$

where  $\omega_{tot} = \omega_i + \omega_e$  is the total volume of the system. When  $f$  is varied, the above expressions for  $\omega_{i/e}$  must be inserted in eqs. (9), (10), (14)–(16) and (19). The surface parameter  $\chi_A$  is varied from 0.1 to 10,  $f$  is varied from 2% to 50%. The standard values of these parameters are

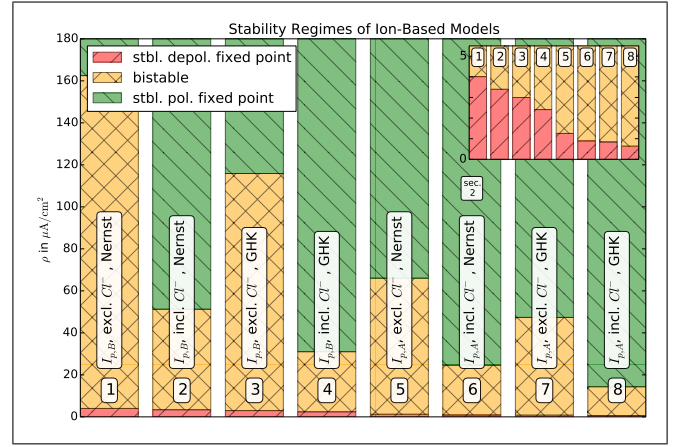


FIG. 4. Overview of the parameter regimes for bistability, polarized and depolarized stability for different models (1–8). The change from the monostable depolarized regime to bistability (red to orange) defines the minimal physiological pump rate, i.e., the pump rate required for the existence of a polarized fixed point. The line separating the bistable from the monostable polarized regime (orange to green) defines the minimal recovery pump rate, i.e., the pump rate required to return from the depolarized fixed point to the polarized equilibrium. Model 6 is used in Sec. 2.

$\chi_A = 1$  and  $f = 25\%$  and parameters are understood to take these values when they are not varied. We start from the bifurcation diagram of fig. 2 and perform two-parameter continuations of the detected bifurcations to find out how the membrane surface and the volume ratio change the bistable regime. The  $(\rho, \chi_A)$ - and  $(\rho, f)$ -continuation curves are shown in the left and right plot of fig. 5.

We see that the  $\chi_A$  variation has hardly any effect on the bifurcation values of  $\rho$ . This can be understood from the structure of the model. The fixed point curve is defined by setting the rate eqs. (2), (9), (10), (13) and the constraint eqs. (6), (7), (14)–(16) and (19) to zero. When  $\chi_A$  is varied the only modification to these conditions is in eq. (19). But this modification is of order  $\mathcal{O}(10^{-5})$  and does practically not affect the shape of the fixed point curve, so the limit point bifurcations LP1 and LP2 are almost not changed. Hopf bifurcation could be shifted, but a rescaling of the (initial and dynamical) ion concentrations by  $\chi_A$  transforms the rate and constraint equations such that  $\chi_A$  only appears in the pump currents. Their derivatives are then multiplied by  $\chi_A$ , but for all HBs the pumps are saturated and hence  $\chi_A$  does not contribute to the Jacobian. The variation of  $f$ , however, does change the width (with respect to  $\rho$ ) and the threshold values of the bistable regime. A small value of  $f$  (corresponding to a small extracellular space) reduces the recovery pump rate, and also increases the minimal physiological pump rate. This means that both, depolarization and recovery, are enhanced. However, the minimal physiological pump rate is much less affected than the recovery pump



TABLE II. Membrane permeabilities for GHK current

name	value & unit	description
$P_{Na}^l$	0.0264 $\mu\text{m}/\text{sec}$	leak sodium permeability
$P_{Na}^g$	150.77 $\mu\text{m}/\text{sec}$	gated sodium permeability
$P_K^l$	0.0169 $\mu\text{m}/\text{sec}$	leak potassium permeability
$P_K^g$	13.488 $\mu\text{m}/\text{sec}$	gated potassium permeability
$P_{Cl}^l$	0.0521 $\mu\text{m}/\text{sec}$	leak chloride permeability

rate, so basically a big cell volume supports recovery from the depolarized state. It is known that in spreading depression (SD), where metastable depolarized states that resemble the upper fixed point of our model occur, the osmotic imbalance of ICS and ECS ion concentrations leads to a water influx that makes the cells swell. Our analysis shows that such a process helps the neuron to return to its physiological equilibrium. Interstitial volume fractions of down to 4% are reported in SD, but even for such extreme volume fractions the recovery pump rate is too high for pump driven recovery of the neuron (see the lowest value for  $\rho_{HB3}$  in the right plot of fig. 5). So also the analysis of different cell geometries confirms that ion homeostasis cannot be provided by  $\text{Na}^+/\text{K}^+$  pumps alone.

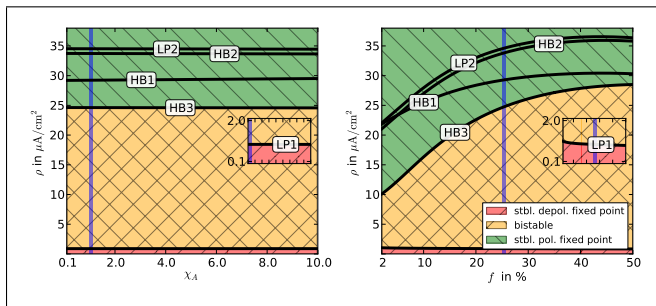


FIG. 5. Two-parameter continuations of the fixed point bifurcations of fig. 2. In the left plot the dimensionless surface size parameter  $\chi_A$  is varied, in the right plot the interstitial volume fraction  $f$  is changed. The insets show the LP1 curves that mark the minimal physiological pump rate. The pump rates for which the system is bistable range from the LP1 to the HB3. The HB3 pump rate is required to repolarize a neuron that is in the depolarized equilibrium. The parameter  $\chi_A$  (left plot plus inset) almost does not change the stability of the system, but  $f$  (right plot) reduces the recovery pump rate significantly. The inset shows that the minimal physiological pump rate is much less affected. In each plot and inset the standard parameter value is indicated by the light-blue vertical line.

## 5. DISCUSSION

Computational neuroscience complements experimental and clinical neuroscience since it can contribute sim-

ulation which help to interpret data and guide a principal understanding of the nervous systems in both health and disease. The HH-formulation of excitability was “so spectacularly successful that, paradoxically, it created an unrealistic expectation for its rapid application elsewhere” as Noble remarked<sup>9</sup>. While his statement refers to modeling of cardiac cells it certainly holds true also for neurological diseases and brain injury<sup>14,16</sup>. In both fields, the incorporation of the  $\text{Na}^+/\text{K}^+$  pump in the original excitability paradigm formulated by Hodgkin and Huxley is of major importance. The fundamental structure of such models has to our knowledge not been exploited in neuroscience beyond merely modulating spiking in epileptiform activity<sup>25,26</sup> or in models that have energy-starved states<sup>17–23</sup> yet without investigating the fundamental bifurcation structure.

As we stressed in the introduction, this extension of the original HH model enforces a physical or rather thermodynamical perspective, which was, of course, the starting point of Hodgkin and Huxley, too. For instance, we also considered the Goldman–Hodgkin–Katz (GHK) current equation which is derived from the constant field assumption applied to the Nernst–Planck equation of electrodiffusion. Electroneutrality is important to consider, as can be seen by the indirect insertion of impermeable counter anions only reflected by observing a thermodynamic Donnan equilibrium. Furthermore, a thermodynamic description of osmotic pressure (which would require a direct insertion of a concentration  $A^{n-}$  of a counter anion with valence  $n$ ) and corresponding changes in cell volume can be included.

Therefore, there are various new quantities that lead to new features in this biophysical ion-based model. At the same time, we have to avoid “an excruciating abundance of detail in some aspects, whilst other important facets [...] can only be guessed”<sup>31</sup>, like using various new currents but guessing the correct value of the valence  $n$  of an impermeable counter anion. For this reason, we decided to use the original ion currents from the HH model, because the basic structure will not be changed by just adding or modifying gating. This question has been addressed experimentally and in simulations by showing that only the simultaneous blockade of all known major cation inward currents did prevent hypoxia-induced depolarization with FES<sup>17,32</sup>. In the model, five different  $\text{Na}^+$  currents were investigated<sup>17</sup>. Of course, to apply our model to a particular pathological condition, like migraine which is a channelopathy<sup>33,34</sup> (disease caused by modified gating), these details will become important. This can easily be incorporated in future investigations. Moreover, note that changes in cell volume, which are very important in brain injuries, are in this study only treated by varying it as a parameter.

Our bifurcation analysis shows that a whole class of minimal ion-based models is bistable for a large range of pump rates ( $\rho_{LP1} < \rho < \rho_{HB3}$ ). Bistable dynamics were suggested by Hodgkin to explain spreading depression, a variant of the more general phenomenon of spread-



ing depolarizations<sup>14,15</sup>, and a corresponding model has been investigated mathematically by Huxley but never been published (cf. Ref.<sup>35</sup>). Dahlem and Müller suggested to extend this ad hoc approach, i.e., a single so-called activator variable with a bistable cubic rate function, by including an inhibitory mechanism in form of an inhibitor species with a linear rate function coupled to the activator<sup>35</sup>. This, of course, leads to the well known FitzHugh–Nagumo paradigm of excitability type II<sup>36,37</sup>, that is, excitability caused by a Hopf bifurcation<sup>38</sup>.

This should not be mistaken as a modification of conductance-based excitability in form of HH-type model in the ‘first generation’ and the interpretation as an equivalent electrical circuit. Dahlem and Müller suggested to use the same mathematical structure of an activator–inhibitor type model<sup>35</sup> to describe a fundamental new physiological mechanism of ion-based excitability originating from bistable ion dynamics. Our current results provide the missing link between this ad hoc activator–inhibitor type model, which has been widely used in migraine and stroke pathophysiology<sup>35,39–48</sup>, and biophysical plausible models. The major result from this link is the new interpretation of the physiological origin of the ad hoc proposed inhibitory variable<sup>35</sup>. We wrongly interpreted the inhibitory variable before as being related to the pump rate<sup>39,41,43,47</sup>.

As our ion-based model shows bistable dynamics, we see it as essentially capturing the activator dynamics of an excitable system and suspect that it can be transformed into such a system by the introduction of a inhibitory process. Vice versa, excitable systems can be reduced to bistable dynamics by singular perturbation methods. Such reductions are referred to as a threshold reduction. From this perspective our model can be interpreted as the threshold reduction of an excitable system, and we conclude that the model still misses an important inhibitory mechanism. Our analysis shows that unlike what we thought before<sup>39,41,43,47</sup>, ion pumps alone are insufficient. If the pump rate is temporarily decreased to less than the minimal physiological rate, the neuron depolarizes, and normal pump activity does not suffice to recover the physiological state. Depending on the particular model the required recovery pump rates range from three times up to more than 30 times the original value. These high values suggest that also more detailed pump models that, for example, include the coupling of the maximal pump rate to oxygen or glucose<sup>23</sup> will not resolve this bistability.

It can, however, also be seen that a regulation of extracellular ion concentrations that mimic glial buffering and coupling to the vasculature in the form an additional term, for example in form of a diffusive coupling to a bath value in extracellular rate equations, will allow only monostability. In a fixed point state, such a coupling forces all buffered extracellular species to assume the respective bath concentrations. There are no two points on the solution branch that share the same extracellular ion concentrations (not shown in figs. 2 and 3).

Hence one fixed point is selected, the other becomes unstable. We consequently suspect that coupling to some bath (glia/vasculature) plays a crucial role in maintaining ion homeostasis and first results confirm that this will lead to an ion-based model that will recover from large perturbations by an excursion in phase space that is characterized by long transient free energy-starvation.

## ACKNOWLEDGMENTS

The authors are grateful for discussions with Jens Dreier on spreading depolarizations, scientific guidance by Michael Guevara on ion-based models in myocytes, and Steven J. Schiff and Nancy Kopell, for various helpful discussions. This work was supported by the Bundesministerium für Bildung und Forschung (BMBF 01GQ1001B, 01GQ1109) within the Bernstein Center of Computational Neuroscience Berlin.

## APPENDIX: HODGKIN–HUXLEY (HH) MODEL

In this section we review the basic features of HH. We comment on two often used reductions of this model and specify the leak currents, which is necessary for the extension towards ion-based modeling. The rate equations for HH read<sup>1</sup>:

$$\frac{dV}{dt} = -\frac{1}{C_m}(I_{Na^+} + I_{K^+} + I_{Cl^-} - I_{app}), \quad (23)$$

$$\frac{dn}{dt} = \frac{n_\infty - n}{\tau_n}, \quad (24)$$

$$\frac{dh}{dt} = \frac{h_\infty - h}{\tau_h}, \quad (25)$$

$$\frac{dm}{dt} = \frac{m_\infty - m}{\tau_m}. \quad (26)$$

The top equation is simply Kirchhoff’s current law for a membrane with capacitance  $C_m$  and membrane potential  $V$ .  $I_{app}$  is an externally applied current that may, for example, initiate voltage spikes. The gating variables  $n$ ,  $h$ , and  $m$  are the potassium activator, sodium inactivator, and sodium activator, respectively. Their dynamics are defined by their voltage-dependent asymptotic values  $x_\infty$  and relaxation times  $\tau_x$  ( $x = n, m, h$ ). These are given by

$$x_\infty = \frac{\alpha_x}{\alpha_x + \beta_x} \quad \text{and}$$

$$\tau_x = \frac{\phi}{\alpha_x + \beta_x} \quad \text{for } x = n, m \text{ and } h.$$

Here  $\phi$  is a common timescale parameter, and the Hodgkin–Huxley exponential functions are

$$\alpha_m = \frac{0.1(V + 30)}{1 - \exp(-(V + 30)/10)}, \quad (27)$$

$$\beta_m = 4 \exp(-(V + 55)/18), \quad (28)$$

$$\alpha_n = \frac{0.01(V + 34)}{1 - \exp(-(V + 34)/10)}, \quad (29)$$

$$\beta_n = 0.125 \exp(-(V + 44)/80), \quad (30)$$

$$\alpha_h = 0.07 \exp(-(V + 44)/20), \quad (31)$$

$$\beta_h = \frac{1}{1 + \exp(-0.1(V + 14))}. \quad (32)$$

The individual ion currents read

$$I_{Na^+} = (g_{Na}^l + g_{Na}^g m^3 h) \cdot (V - E_{Na}), \quad (33)$$

$$I_{K^+} = (g_K^l + g_K^g n^4) \cdot (V - E_K), \quad (34)$$

$$I_{Cl^-} = g_{Cl}^l \cdot (V - E_{Cl}), \quad (35)$$

with  $g_{ion}^{l,g}$  denoting leak and gated conductances. In fact, Hodgkin and Huxley set up their model with an unspecified leak current and non-leaking sodium and potassium channels. As long as ion dynamics are not considered this is mathematically equivalent to specifying the leak current as being partially sodium, potassium and chloride, but it is physically inconsistent because the reversible potentials for the ions differ. In an ion-based approach, however, the main task of the ion pumps under physiological conditions is to compensate for sodium and potassium leak currents (see Sec. 2) while gated currents are extremely small in the equilibrium. So at this point leak currents for all ion species are important.

The Nernst potentials  $E_{ion}$  are given in terms of the ion concentrations  $[ion]$  in the intracellular space (ICS) and the extracellular space (ECS) denoted by subscripts  $i$  and  $e$ , respectively:

$$E_{ion} = \frac{26.64 \text{mV}}{z_{ion}} \ln([ion]_e/[ion]_i). \quad (36)$$

for  $ion = K, Na$ , and  $Cl$  and  $z_{ion}$  is the ion valence. All model parameters are listed in tab. III. For better readability we omit the square brackets on the ion concentrations and simply write  $K_{i/e}$ ,  $Na_{i/e}$ , and  $Cl_{i/e}$ .

For  $I_{app} = 0$  this model is monostable with an equilibrium at  $V = -68$  mV. Note that  $E_{Na} \neq V$  and  $E_K \neq V$  imply that under equilibrium conditions neither  $I_{Na^+}$  nor  $I_{K^+}$  vanish, but only their sum does. Sufficiently strong current pulses can—depending on their duration—initiate single voltage spikes or spike trains. Constant applied currents can drive the system to a regime of stationary oscillations. The minimal current required for this is usually called rheobase current.

The HH model can be reduced to two dynamical variables in a way that preserves these dynamical features. One common simplification<sup>49</sup> is to eliminate the fastest gating variable  $m$  adiabatically and set

$$m = m_\infty(V). \quad (37)$$

TABLE III. Model parameters for HH

Name	Value & unit	Description
$C_m$	1 $\mu$ F/cm <sup>2</sup>	membrane capacitance
$\phi$	3/msec	gating timescale parameter
$g_{Na}^l$	0.0175 mS/cm <sup>2</sup>	sodium leak conductance
$g_{Na}^g$	100 mS/cm <sup>2</sup>	max. gated sodium conductance
$g_K^l$	0.05 mS/cm <sup>2</sup>	potassium leak conductance
$g_K^g$	40 mS/cm <sup>2</sup>	max. gated potassium conductance
$g_{Cl}^l$	0.05 mS/cm <sup>2</sup>	chloride leak conductance
$Na_i$	27 mMol/l	ECS sodium concentration
$Na_e$	120 mMol/l	ICS sodium concentration
$K_i$	130.99 mMol/l	ECS potassium concentration
$K_e$	4 mMol/l	ICS potassium concentration
$Cl_i$	9.66 mMol/l	ECS chloride concentration
$Cl_e$	124 mMol/l	ICS chloride concentration
$E_{Na}$	39.74mV	sodium Nernst potential
$E_K$	-92.94 mV	potassium Nernst potential
$E_{Cl}$	-68 mV	chloride Nernst potential

Second, there is an approximate functional relation between  $h$  and  $n$  that is usually realized as a linear fit<sup>50</sup>. The ion-based model presented in this article, however, contains a stable fixed point with large  $n$ , and a linear best fit would then lead to a negative  $h$ . Therefore we will use the following sigmoidal fit to make sure  $h$  is non-negative:

$$h = h_{sig}(n) = 1 - \frac{1}{1 + \exp(-6.5(n - 0.35))}. \quad (38)$$

After this reduction the remaining dynamical variables are  $V$  and  $n$ .

## REFERENCES

- 1A. L. Hodgkin and A. F. Huxley, “A quantitative description of membrane current and its application to conduction and excitation in nerve,” *J. Physiol.* **117**, 500 (1952).
- 2M. Beilby and H. Coster, “The action potential in chara corallina iii.\* the hodgkin-huxley parameters for the plasmalemma,” *Functional Plant Biology* **6**, 337–353 (1979).
- 3L. Ebihara and E. Johnson, “Fast sodium current in cardiac muscle. a quantitative description,” *Biophysical journal* **32**, 779–790 (1980).
- 4T. R. Chay and J. Keizer, “Minimal model for membrane oscillations in the pancreatic beta-cell,” *Biophys. J.* **42**, 181–190 (1983).
- 5I. Atwater, C. M. Dawson, A. Scott, G. Eddlestone, and E. Rojas, “The nature of the oscillatory behaviour in electrical activity from pancreatic beta-cell,” *Horm. Metab. Res. Suppl.* **Suppl 10**, 100–107 (1980).
- 6C. Y. Cha, Y. Nakamura, Y. Himeno, J. Wang, S. Fujimoto, N. Inagaki, Y. E. Earm, and A. Noma, “Ionic mechanisms and Ca2 dynamics underlying the glucose response of pancreatic  $\beta$  cells: a simulation study,” *J. Gen. Physiol.* **138**, 21–37 (2011).
- 7D. DiFrancesco and D. Noble, “A model of cardiac electrical activity incorporating ionic pumps and concentration changes,”

- Philosophical Transactions of the Royal Society of London. B, Biological Sciences **307**, 353–398 (1985).
- <sup>8</sup>S. Dokos, B. Celler, and N. Lovell, “Modification of difrancesconoble equations to simulate the effects of vagal stimulation onin vivo mammalian sinoatrial node electrical activity,” *Annals of biomedical engineering* **21**, 321–335 (1993).
- <sup>9</sup>D. Noble and Y. Rudy, “Models of cardiac ventricular action potentials: iterative interaction between experiment and simulation,” *Philosophical Transactions of the Royal Society of London. Series A: Mathematical, Physical and Engineering Sciences* **359**, 1127–1142 (2001).
- <sup>10</sup>A. Varghese and G. R. Sell, “A conservation principle and its effect on the formulation of Na-Ca exchanger current in cardiac cells,” *J. Theor. Biol.* **189**, 33–40 (1997).
- <sup>11</sup>L. Endresen, K. Hall, J. Høyve, and J. Myrheim, “A theory for the membrane potential of living cells,” *European Biophysics Journal* **29**, 90–103 (2000).
- <sup>12</sup>C. Y. Cha, Y. Himeno, T. Shimayoshi, A. Amano, and A. Noma, “A novel method to quantify contribution of channels and transporters to membrane potential dynamics,” *Biophys. J.* **97**, 3086–3094 (2009).
- <sup>13</sup>H. Arce, A. Xu, H. González, and M. R. Guevara, “Alternans and higher-order rhythms in an ionic model of a sheet of ischemic ventricular muscle,” *Chaos: An Interdisciplinary Journal of Non-linear Science* **10**, 411–426 (2000).
- <sup>14</sup>J. P. Dreier, “The role of spreading depression, spreading depolarization and spreading ischemia in neurological disease,” *Nat. Med.* **17**, 439–447 (2011).
- <sup>15</sup>A. C. Charles and S. M. Baca, “Cortical spreading depression and migraine,” *Nat. Rev. Neurol.* (2013).
- <sup>16</sup>J. P. Dreier, T. M. Isele, C. Reiffurth, S. A. Kirov, M. A. Dahlem, and O. Herreras, “Is spreading depolarization characterized by an abrupt, massive release of Gibbs free energy from the human brain cortex?” *Neuroscientist* **19**, 25–42 (2013).
- <sup>17</sup>H. Kager, W. J. Wadman, and G. G. Somjen, “Simulated seizures and spreading depression in a neuron model incorporating interstitial space and ion concentrations,” *J. Neurophysiol.* **84**, 495–512 (2000).
- <sup>18</sup>B. E. Shapiro, “Osmotic forces and gap junctions in spreading depression: a computational model,” *J. Comput. Neurosci.* **10**, 99–120 (2001).
- <sup>19</sup>R. M. Miura, H. Huang, and J. J. Wylie, “Cortical spreading depression: An enigma,” *Eur. Phys. J. Spec. Top.* **147**, 287–302 (2007).
- <sup>20</sup>G. G. Somjen, H. Kager, and W. J. Wadman, “Computer simulations of neuron-glia interactions mediated by ion flux,” *J. Comput. Neurosci.* **25**, 349–365 (2008).
- <sup>21</sup>G. Florence, M. A. Dahlem, A. C. G. Almeida, J. W. M. Bassani, and J. Kurths, “The role of extracellular potassium dynamics in the different stages of ictal bursting and spreading depression: A computational study,” *J. Theor. Biol.* **258**, 219 (2009).
- <sup>22</sup>B. J. Zandt, B. ten Haken, J. G. van Dijk, and M. J. van Putten, “Neural dynamics during anoxia and the ”wave of death”,” *PLoS ONE* **6**, e22127 (2011).
- <sup>23</sup>J. C. Chang, K. C. Brennan, D. He, H. Huang, R. M. Miura, P. L. Wilson, and J. J. Wylie, “A mathematical model of the metabolic and perfusion effects on cortical spreading depression,” *PLoS ONE* **8**, e70469 (2013).
- <sup>24</sup>J. Cham, *Abstract Mad Libs* (Piled Higher and Deeper, 2009).
- <sup>25</sup>J. R. Cressman Jr., G. Ullah, J. Ziburkus, S. J. Schiff, and E. Barreto, “The influence of sodium and potassium dynamics on excitability, seizures, and the stability of persistent states: I. single neuron dynamics,” *J. Comput. Neurosci.* **26**, 159–170 (2009).
- <sup>26</sup>E. Barreto and J. R. Cressman, “Ion concentration dynamics as a mechanism for neural bursting,” *J. Biol. Phys.* **37**, 361–373 (2010).
- <sup>27</sup>N. Yu, C. E. Morris, B. Joos, and A. Longtin, “Spontaneous excitation patterns computed for axons with injury-like impairments of sodium channels and Na/K pumps,” *PLoS Comput. Biol.* **8**, e1002664 (2012).
- <sup>28</sup>P. A. Boucher, B. Joós, and C. E. Morris, “Coupled left-shift of nav channels: modeling the na -loading and dysfunctional excitability of damaged axons,” *J. Comp. Neurosci.* , 1–19 (2012).
- <sup>29</sup>K. Aihara and G. Matsumoto, “Two stable steady states in the Hodgkin-Huxley axons,” *Biophys. J.* **41**, 87–89 (1983).
- <sup>30</sup>Y. A. Kuznetsov, *Elements of Applied Bifurcation Theory* (Springer, New York, 1995).
- <sup>31</sup>R. M. May, “Uses and abuses of mathematics in biology,” *Science* **303**, 790–793 (2004).
- <sup>32</sup>M. Muller and G. G. Somjen, “Inhibition of major cationic inward currents prevents spreading depression-like hypoxic depolarization in rat hippocampal tissue slices,” *Brain Res.* **812**, 1–13 (1998).
- <sup>33</sup>S. Silberstein and D. Dodick, “Migraine Genetics - A Review: Part I,” *Headache* (2013).
- <sup>34</sup>S. D. Silberstein and D. W. Dodick, “Migraine Genetics: Part II,” *Headache* (2013).
- <sup>35</sup>M. A. Dahlem and S. C. Müller, “Reaction-diffusion waves in neuronal tissue and the window of cortical excitability,” *Ann. Phys.* **13**, 442–449 (2004).
- <sup>36</sup>R. FitzHugh, “Impulses and physiological states in theoretical models of nerve membrane,” *Biophys. J.* **1**, 445–466 (1961).
- <sup>37</sup>J. Nagumo, S. Arimoto, and S. Yoshizawa, “An active pulse transmission line simulating nerve axon.” *Proc. IRE* **50**, 2061–2070 (1962).
- <sup>38</sup>G. B. Ermentrout, “Neural networks as spatio-temporal pattern-forming systems,” *Rep. Prog. Phys.* **61**, 353–430 (1998).
- <sup>39</sup>M. A. Dahlem, F. M. Schneider, and E. Schöll, “Efficient control of transient wave forms to prevent spreading depolarizations,” *J. Theo. Biol.* **251**, 202–209 (2008).
- <sup>40</sup>M. A. Dahlem, F. M. Schneider, and E. Schöll, “Failure of feedback as a putative common mechanism of spreading depolarizations in migraine and stroke,” *Chaos* **18**, 026110 (2008).
- <sup>41</sup>M. A. Dahlem and N. Hadjikhani, “Migraine aura: retracting particle-like waves in weakly susceptible cortex,” *PLoS ONE* **4**, e5007 (2009).
- <sup>42</sup>D. E. Postnov, F. Müller, R. B. Schuppner, and L. Schimansky-Geier, “Dynamical structures in binary media of potassium-driven neurons,” *Phys. Rev. E* **80**, 031921 (2009).
- <sup>43</sup>M. A. Dahlem, R. Graf, A. J. Strong, J. P. Dreier, Y. A. Dahlem, M. Sieber, W. Hanke, K. Podoll, and E. Schöll, “Two-dimensional wave patterns of spreading depolarization: retracting, re-entrant, and stationary waves,” *Physica D* **239**, 889–903 (2010).
- <sup>44</sup>F. M. Schneider, E. Schöll, and M. A. Dahlem, “Controlling the onset of traveling pulses in excitable media by nonlocal spatial coupling and time delayed feedback,” *Chaos* **19**, 015110 (2009).
- <sup>45</sup>M. A. Dahlem and T. M. Isele, “Transient localized wave patterns and their application to migraine,” *J. Math. Neurosci* **3**, 7 (2013).
- <sup>46</sup>D. E. Postnov, D. D. Postnov, and L. Schimansky-Geier, “Self-terminating wave patterns and self-organized pacemakers in a phenomenological model of spreading depression,” *Brain Res.* **1434**, 200–211 (2012).
- <sup>47</sup>M. A. Dahlem, “Migraine generator network and spreading depression dynamics as neuromodulation targets in episodic migraine,” *Chaos* (accepted) (2013).
- <sup>48</sup>M. A. Dahlem, S. Rode, A. May, N. Fujiwara, Y. Hirata, K. Aihara, and J. Kurths, “Towards dynamical network biomarkers in neuromodulation of episodic migraine,” *Transl. Neurosci.* **4**, 282–294 (2013).
- <sup>49</sup>J. Rinzel and G. B. Ermentrout, “Analysis of neural excitability and oscillations,” in *Methods in neuronal modeling*, edited by C. Koch and I. Segev (MIT Press, Cambridge, MA, 1989) pp. 251–291.
- <sup>50</sup>G. B. Ermentrout and D. Terman, *Mathematical Foundations of Neuroscience* (Springer, 2010).